Physical Modelling in Geotechnics

Observation of ground behavior during pile loading test in centrifuge by particle image velocimetry (PIV)

T. Kiriyama, Y. Zhou, & Y. Asaka
Institute of technology, Shimizu corporation, Tokyo, Japan

ABSTRACT: The authors have performed a series of centrifugal experiments focusing on pile-end resistance and the area of ground resistance around the pile end. There are existing theories that explain these behaviors, but none have ever been verified in an actual stress field. In these experiments, ground behavior during pile loading/uplift is captured using a modern high-resolution 4K (8 mega pixels) digital camera and the resulting images are processed by Particle Image Velocimetry (PIV). Images captured during centrifugal experiments often suffer from noise due to mechanical vibration, causing difficulty in understanding primary deformations such as strain localization when processed using PIV. The authors develop a pre-processing method that is able to expose strain localization. Through the resulting visualization of strain localization, it is revealed that the area of ground resistance around a pile grows progressively in two stages, both during loading and uplift: primary bulbs of resistance first arise around the pile, and this is followed by the subsequent development of secondary bulbs.

Keywords: Particle image velocimetry, Centrifugal modelling, Pile loading test

1 INTRODUCTION

Pile-end bearing capacity is one of the classical problems in which practical engineering proceeds based on the basis of theoretical failure patterns that have not been verified by observation. Figure 1(a) shows ground failure patterns around a loaded pile end according to the classical theories (Bishop et al. 1945; Meyerhof 1951; Reissner 1924; Vesić 1963). Figure 1(b) shows ground failure patterns around the belled part of an expanded pile in uplift, as based on proposed theories (Clemence and Veesaert 1977; Down and Chieuzzi 1966; Majer 1955; Meyerhof and Adams 1968; Murray and Geddes 1987; Sutherland et al. 1982; Vermeer and Sutjiadi 1985). Even though these theories predict ground failure patterns around a pile end or bell, their predictions have not been verified by observation of ground deformation under an actual confining stress field, a condition in which a geomaterial behaves completely differently than when under low confining stress because its characteristics are confining-stress dependent. The conventional theories are able to explain experimental measurements, but this does not mean that actual ground failure occurs in the proposed patterns, because this has yet to be confirmed by observation for either pile loading or uplift.

The authors set out to observe ground behavior during pile loading/uplift under an actual stress field by performing pile loading experiments in a centrifuge as a way to realize an actual confining stress field. In this paper, the experimental setup and the use of Particle Image Velocimetry (PIV) are reported for the physical models of pile loading/uplift, and the ground resisting areas in pile loading/uplift are discussed.

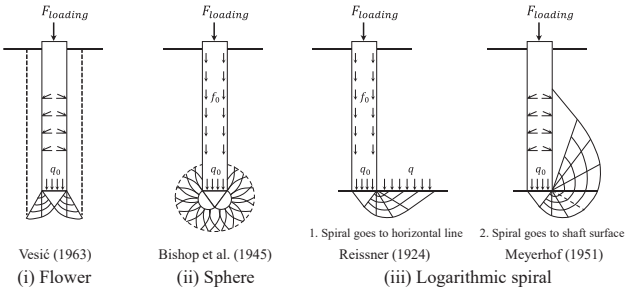

(a) Pile loading (Victor 1969)

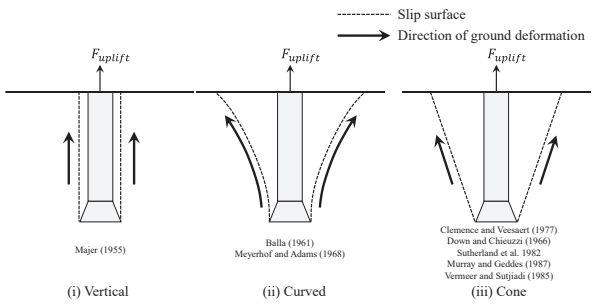

(b) Pile uplift

Fig. 1. Ground resisting areas in pile loading/uplift

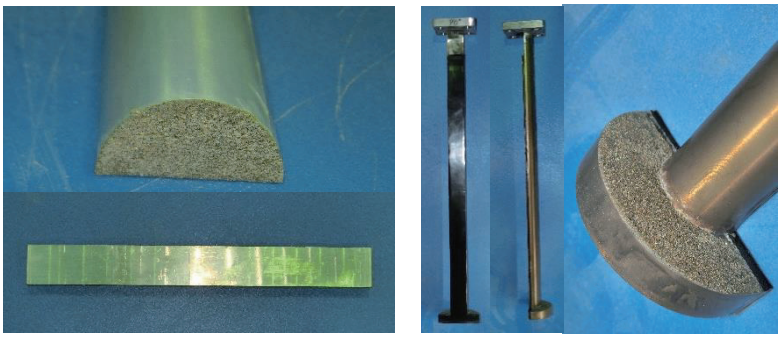

(a) (b)

Photo 1. Model pile for loading/uplift experiments. (a) Loading pile half model; (b) Uplift pile half model

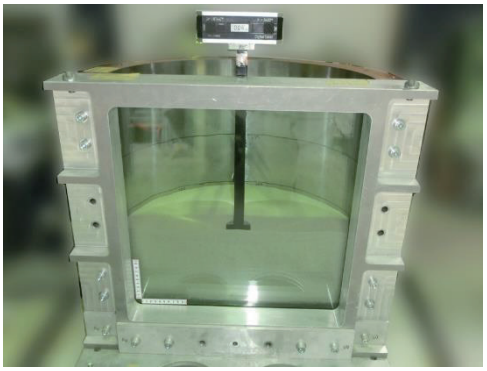

Photo 2. Half-cylinder container with observation window for ground deformation

2 PILE LOADING IN CENTRIFUGE

Performing pile loading in a centrifuge requires careful preparation because centrifugal experiments are basically a kind of downsized version of tests on actual structures. Modeling errors are easily introduced because any errors are multiplied by the law of similarity. In order to confirm the experimental integrity, all tests described here have been performed at least twice to prove the reproductivity of the observed results.

In this series of experiments centrifugal acceleration is fixed at 60g. All sizes are described below in model scale followed by prototype scale.

2.1 Pile and container specifications

Photo 1 shows the pile models used for loading/uplift experiments. The loading pile (Photo 1(a)) is a straight cylinder with a diameter of 4cm (2.4m in prototype, b_b), while the uplift pile (Photo 1(b)) has an anchor plate at the bottom; the shaft is 2cm (1.2m, b_s) in diameter and the plate 5cm (3m, b_b). Half models of the piles are used to allow for observation through a window. In order to avoid friction against the observation window, the cut section of the loading pile is covered with Teflon sheet, while the uplift pile is covered with 2mm of polyurethane followed by polyethylene sheet. Toyoura sand ($D_{50} = 0.196$mm) is bonded to the bottom of the straight pile and to the upper side of the anchor plate of the uplift pile. For both types of pile, the shaft is wrapped with Teflon to eliminate skin friction because the focus in this series of experiments is on ground resistance against the pile end.

The rigid container (soil box) consists of half a steel cylinder 50cm (30m) in diameter and 50cm (30m) in height, and fitted with an observation window on the open side. The model ground is prepared by the air pluviation method, in which the base ground of 20cm (12m) depth is prepared at first. The model piles are then placed in position against the observation window and finally the upper ground of 25cm (15m) depth is prepared. This simulates on-site cast-in-place pile installation. Toyoura sand under dry dense conditions is used for the model ground (D_r = 90% or more; $\rho_d = 1.63\ g/cm^3$).

2.2 Centrifuge and pile loading device

The centrifuge, which has 3.1m arms, is capable of 100g centrifugal loading under the static loading condition. The container and a gate-type loading jack are fixed to a stage attached at the end of the centrifuge arm. The jack is electrically controlled to provide a loading rate of 0.2mm/min, and has a capacity of 5tf loading and 100mm stroke. A load-cell and a laser displacement meter are used to measure the load-displacement relationship at the pile head. Bender elements are also set at the depth of the pile end to confirm that model grounds are prepared with the target property.

2.3 Photographic observations

A digital camera with 4K resolution (8 mega pixels) is used for photography. It is fixed to the steel frame adjacent to the observation window. Photo 3 shows the experimental setup just before centrifugal loading. Photography is programed to start at a specific time and

Photo 3. 4K digital camera is set at the side of the observation window.

capture images at specific intervals; in this series of experiments, image capture is delayed for 20 min while the centrifugal force increases, and the image capture interval is 5 seconds.

3 PIV FOR CENTRIFUGAL GROUND DEFORMATION

PIV analysis itself has been widely applied to problems of ground deformation (e.g., White et al. 2003), along with X-ray tomography which is also used to visualize deformation (Otani et al. 2006). However, to date, PIV observation experiments have been often performed under normal gravity (1g) or with quite a small confining stress field; these conditions do not simulate the actual behavior of ground subjected to much higher confining stress fields. It should be noted that a geomaterial under 1g in a downsized model shows too much dilatancy, leading to misunderstanding of ground behavior. This series of experiments is performed to apply the PIV technique to observations in a centrifuge for the purpose of analyzing ground behavior around piles under an actual confining stress field.

3.1 Pre-processing of captured images

PIV analysis of images captured in a centrifuge is often difficult to perform because capture equipment vibrates during the experiments, leading to a lot of noise in the captured images. It is necessary to improve the original images by appropriate pre-processing for better visualization. The authors have developed the visualization method in which the vibration noise is eliminated while the deformations (strains) are clearly visualized by optimizing the brightness of images, in which the displacements are kept the same as they were from the original brightness images while only the areas with intensive deformation are detected in the following imaging process.

3.2 Imaging of deformation

PIV analysis begins with setting the image at zero displacement as the origin, and displacement vectors between the origin and the target image are analyzed. The PIV inspection window is sized at 8x8 pixels, where each pixel is equivalent to about 0.15mm. The load-displacement results and photography are synchronized at the point when contact is made between the pile head and the loading plate. The moment of contact is recognized in the load cell measurements as the point when the load rises instantaneously due to contact. With this preparation, PIV analysis can be used to calculate ground displacements. The authors focus further on the deformation (strain) of the ground because slip lines are generated as ground deforms. Maximum shear strains (γ_{max}) are calculated from the displacement vector by using a quadrilateral shape function, in which the PIV inspection window is treated as a quadrilateral.

4 IMAGING OF GROUND RESISTANCE AREA IN PILE LOADING/UPLIFT

The PIV analysis discussed here focuses on the areas of ground resistance during pile loading/uplift under an actual confining stress field.

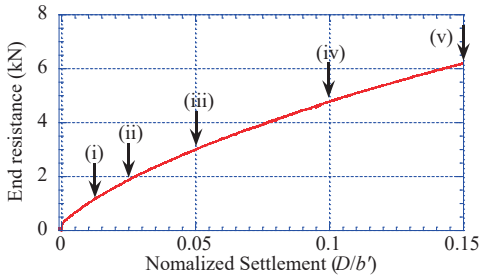

(a) Pile loading; (i)-(v) are (a)-(e) in Fig. 3.

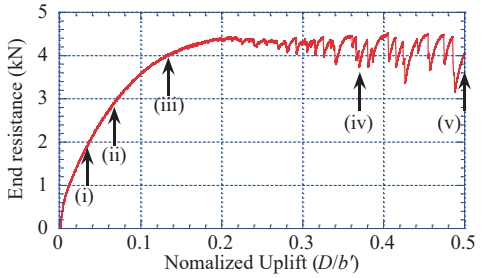

(b) Pile uplift; (i)-(v) are (a)-(e) in Fig. 4.

Fig. 2. Load-displacement relationship

4.1 Ground behavior during pile loading

Figure 2(a) and Fig. 3 show the load-displacement curve for the pile end and distributions of maximum shear strain during pile loading, respectively. The normalized uplift is obtained by dividing the uplift(D) by effective pile-end diameter ($b' = b_b$ in pile loading). b' is the effective part of a pile diameter that transports external load directly to the ground around pile end. The range of ground resisting areas are also described as L_x and L_y in both horizontal and vertical direction against the effective pile-end diameter. Pile-end resistance continuously rises in Fig. 2(a) while at the same time the area of resistance, as demarcated by the maximum shear strain, expands from (a) to (e) in Fig. 3. The widening area of resistance explains the continuous increase in end resistance seen in Fig. 2(a). Looking at the detail in Fig. 3 as the area of resistance grows, it can be seen that: 1) primary bulbs of resistance repeatedly arise from the bottom of the pile; 2) secondary bulbs are subsequently initiated at the punching wedge beneath the pile bottom; 3) subsidiary relaxation occurs around the pile shaft due to settlement of the ground around the pile end. The ground resisting area ranges almost the same in horizontal and vertical direction until $D/b' = 0.025$, while it becomes wider horizontally after $D/b' = 0.025$.

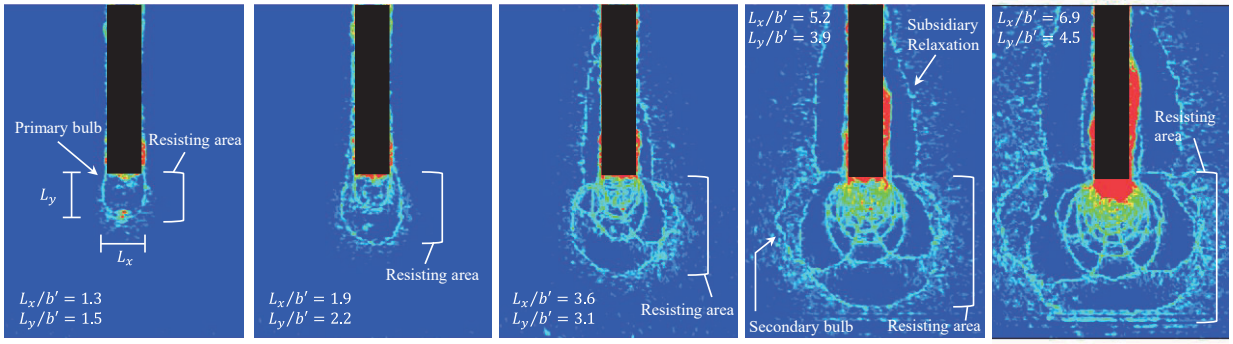

(a) D/b'=0.0125 (b) D/b'=0.025 (c) D/b'=0.05 (d) D/b'=0.1 (e) D/b'=0.15

Fig. 3. Maximum shear strain (γ_{max}) distribution during pile loading at each stage of settlement

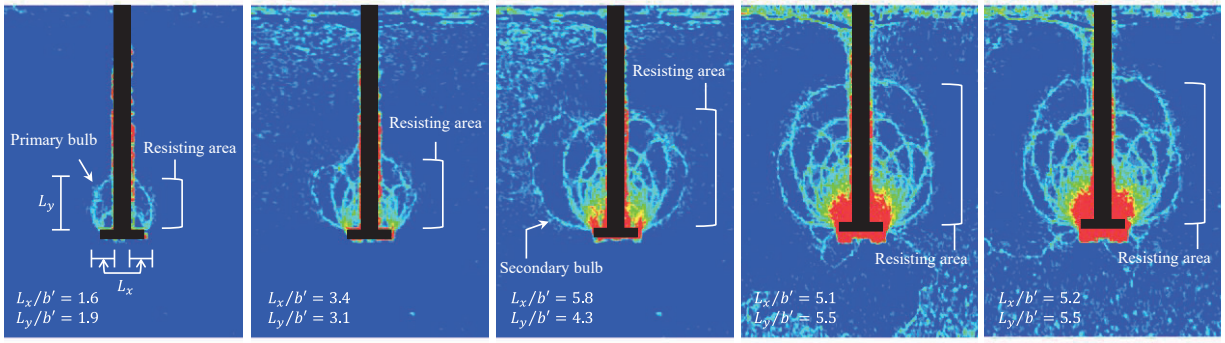

(a) D/b'=0.03 (b) D/b'=0.07 (c) D/b'=0.13 (d) D/b'=0.36 (e) D/b'=0.5

Fig. 4. Maximum shear strain (γ_{max}) distribution during pile uplift at each stage of uplift

4.2 Ground behavior during pile uplift

Figure 2(b) and Fig. 4 show the load-displacement curve and the distributions of maximum shear strain during pile uplift, respectively ($b' = b_b - b_s$ in pile uplift). Pile-end resistance rises until reaching an ultimate state at uplift $D/b' = 0.36$, while the strain distribution remains unchanged beyond this point, meaning the area of ground resistance explains the end resistance. As in the pile loading case, the area of ground resistance grows progressively, with primary bulbs generated first, followed by secondary bulbs.

5 CONCLUSIONS

The areas of ground resistance during both pile loading and uplift have been observed in an actual stress field through centrifuge experiments, and the following PIV, in which the captured images were processed with the brightness optimization. The visualized strain distributions explain that, in both loading/uplift conditions, the areas of ground resistance grow progressively in two stages. First, primary bulbs of resistance form around the pile, and this stage is followed by the subsequent development of secondary bulbs.

REFERENCES

Bishop, R.F., Hill, R., and Mott, N.F. 1945. The theory of indentation and hardness tests. *Proceedings of the Physical Society* 57, 147–159.

Clemence, S.P., and Veesaert, C.J. 1977. Dynamic pullout resistance of anchors in sand, *Proceedings of international symposium on soil structure interaction*, *Roorkee*, *India*, 389-397.

Down, D.I., and Chieurzzi, R. 1966. Transmission tower foundations, *ASCE Journal of the Power Division* 92 (P02), 91-114.

Majer, J., Zur Berechnung von Zugfundamenten 1955. *Osterreichische Bauzeitschrift* 10 (5), 85-90. (in German)

Meyerhof, G.G. 1951. The ultimate bearing capacity of foundations. Géotechnique, 2(4) 301–332.

Meyerhof, G.G., and Adams, J.I. 1968. The ultimate uplift capacity of foundations, *Canadian Geotechnical Journal* 5 (4) 225-244.

Murray, E.J., and Geddes, J.D. 1987. Uplift of anchor plates in sand, *ASCE Journal of Geotechnical Engineering*, 113 (3).

Otani, J., Pham, K.D., and Sano, J. 2006. Investigation of failure patterns in sand due to laterally loaded pile using X-ray CT, *Soils and foundations*, 46 (4) 529-535.

Reissner, H. 1924. Zum Erddruck problem. *Proceedings of the 1st International Congress of Applied Mechanics*, Delft, The Netherlands, 22–26 April 1924. Edited by C.B. Biezeno and J.M. Burgers. 295–311. [In German.]

Sutherland, H.B., Finilay, T.W., and Fadl, M.O. 1982. Uplift capacity of embedded anchors in sand, *Proceedings of 3rd international conference on the behavior of offshore structures*, *Cambridge*, *MA* (2), 451-463.

Vermeer, P.A., and Sutjiadi, W. 1985. The uplift resistance of shallow embedded anchors, *Proceedings of 11th international conference on soil mechanics and foundation engineering*, *San Francisco*, *CA*, (4) 1635-1638.

Vesić, A.S. 1963. Bearing capacity of deep foundations in sand, *Highway Research Record* 39: 112–153.

Victor, F.B. 1969. Foundations of buildings in clay, state of the art report, 7th international conference on soil mechanics and foundation engineering, Mexico.

White, D.J., Take, W.A. and Bolton, M.D. 2003. Soil deformation measurement using particle image velocimetry (PIV) and photogrammetry, Géotechnique 53 (7), 619-631.